Fano Resonance in Quantum Metamaterials

by Ahmad Ali Khan

Submission date: 28-Feb-2024 09:09PM (UTC-0800)
Submission ID: 2307657201
File name: Fano_Resonance_in_Quantum_Metamaterials__2__2.pdf (376.75K)
Word count: 6076
Character count: 32103

Chapter 1

Introduction

In the early 2000s, scientists began experimenting with creating materials that could perform tasks not found in nature.By manipulating electromagnetic waves using artificial structures, they successfully developed a new class of materials called metamaterials[**?**] These materials exhibit extraordinary properties for manipulating light. Such as making things disappear or capture incredibly detailed images. These materials are called metamaterials.But now, scientists are taking the materials to a whole new level by adding super tiny quantum elements, creating something they call Quantum Metamaterials. The Quantum Metamaterials, made up of quantum elements have specific quantum states which keep those states working together for a really long time. This is crucial for advanced technologies in fields like quantum sensing and information processing[**?**].The development of such materials entails exploring their suitability for quantum information processing. An intriguing experiment entails integrating quantum emitters into a negative permeability metamaterial configuration. This essentially means adding tiny light-emitting particles to enhance the material's responsiveness[**?**]. In this study, we investigate the incorporation of quantum emitters into a metamaterial framework with negative permeability, thereby enabling the manipulation of tunability and nonlinear characteristics. Our metamaterial's nano hybrid molecule, composed of metal nanoparticles and semiconductor quantum dots (SQDs). In the absence of SQDs, the nano hybrid molecule's ring functions as an artificial optical magnetic resonator. The introduction of SQDs induces a Fano inter-

ference profile, significantly impacting the collective magnetic resonance.This interference becomes a tool to fine-tune the negative permeability metamaterial response.Moreover, by delving into the intrinsic nonlinearity of quantum dots (QDs), we suggest manipulating the magnetic response of the metamaterial through the introduction of a distinct control field. Additionally, employing a quantized approach, we conduct theoretical analyses on the optical attributes of a hybrid system comprising metal nanoparticles and quantum dots under the influence of an external laser field. This investigation unveils controlled resonance fluorescence features. The method's versatility extends to other nanoscopic structures, presenting potential applications in advanced technologies [**?**].

Nanoparticles : A super small tiny particles, usually of 1 to 100 nanometers in size. They have special properties because of their size. We may imagen them as really tiny spheres made of material atoms.

Moreover MNPs are made of metals like gold or silver, Where as semiconductor nanoparticles are made of materials like InAs or CdS. In cause semiconductor nano particles trap an electron and a hole (a missing electron) in all directions, they're called SQDs.

In this study, we're looking at metallic nanoparticles ranging from a few nanometers to 100 nm. Because there are lots of electrons in these metals, we can think of them like tiny classical objects. The slightly smaller SQDs, on the other hand, need a more quantum approach for modeling because of how electrons are confined inside them.

Nano-Super-Structures : A bunch of really tiny things grouped together is called a nanosuperstructure. These small-scale setups have special abilities and can be designed for specific tasks. Thanks to progress in nanoscience, we can now create and study these nanosuperstructures by combining different building blocks like nanowires, quantum dots etc. This lets us explore science that range from classical to quantum mechanics. It's not just about understanding the science; these structures might lead to new devices in quantum information technology. Imagine being able to move excitations and coherent states around!

Experiments have shown that we can control where quantum dots land

near nanowires using a cool process. We've also put together hybrid structures, like quantum dots connected to metal nanoparticles through biolinkers. This combo showed efficient conversion of excitons, plasmons, and photons, leading to enhanced emission rates.

One exciting area is combining semiconductor quantum dots (SQDs) with metal nanoparticles (MNPs). This mix is a hot topic in theoretical physics because it lets us study systems that blend classical and quantum physics. It could even open doors to sending tiny bits of information and excitations in a specific direction.

In this thesis, we're diving into the physics of nanohybrid molecules, specifically those made with MNP and SQDs. We want to see how a nearby quantum dot influences the behavior of a metal nanoparticle. By understanding how these tiny particles act together, we're unlocking new possibilities in science and technology.

Application : Quantum Hybrid Controllable Metamaterials offer diverse applications, including biosensors and medical imaging in Sensing Technology [**?**], potential invisibility in Cloaking Devices [**?**], and superlenses overcoming diffraction limits. Tailored for Energy Harvesting, they convert specific electromagnetic frequencies into usable energy [**?**]. In Communications, these metamaterials enhance signal processing and wireless technologies, while in Optical Devices [**? ?**], they focus different wavelengths for advanced imaging. Acoustic Metamaterials control sound waves for noise reduction, ultrasound imaging, and seismic wave mitigation [**?**]. In Quantum Computing, quantum metamaterials contribute to developing qubits and controlling quantum states, showcasing their versatile potential across various technological domains [**?**]. Ongoing research continues to uncover new possibilities, making this field dynamic and promising.

Chapter 2

Hybrid Nano - Structure

As illustrated in the schematic diagram shown in Figure 2.1, we examine a hybrid structure that consists of a two-level QD and a spherical MNP with a radius denoted as r_m . Positioned at a center-to-center distance marked as d, the MNP and QD are immersed in a uniform dielectric medium characterized by a permittivity denoted as ϵ_b. This hybrid molecule is exposed to both an external driving field $E_{dri} = E_0 e^{-\iota\omega_d t} + c.c.$ where E_0 represents the amplitude, ω_d is the angular frequency, and c.c. indicates the complex conjugation. Additionally, it experiences the influence of a broadband squeezed vacuum denoted as E_{squ}. The polarization of the externally applied electric field aligns with the axis connecting the MNP and QD structure.[12]

The MNP possesses remarkable optical characteristics, allowing it to sustain LSPs. This capability enables the MNP to amplify and concentrate optical fields into subwavelength ranges [13]. In the case of plasmonic metals with a single valence (such as silver, gold, copper, and alkaline metals), the skin depth (l_s) for these metals is approximately 25 nm across the entire optical spectrum [14].For MNP such a small scale where the $r_m \leq l_s$, the external light field has the capability to permeate the entire MNP. This penetration induces collective electron oscillations, allowing the MNP to confine electromagnetic energy in the form of electromechanical energy at the nanoscale. When the size of the MNP is significantly smaller than the wavelength (λ) of the incident light ($r_m \ll \lambda$), (it becomes evident that the condition $r_m \ll \lambda$ is inherently met, especially when $r_m \leq l_s$). The quasistatic approximation proves to be a

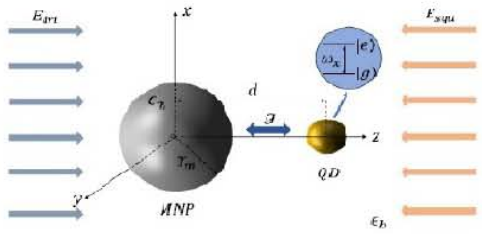

Figure 2.1: Illustration of the hybrid system consisting of a spherical MNP and a QD embedded in a homogeneous dielectric medium with a relative permittivity of ϵ_b (in this case, vacuum, $\epsilon_b = 1$). Both the MNP and the two-level QD are subjected to an external electric field E_{dri}. To clarify the polarization direction of the applied electric field, we define the major axis of the hybrid MNP-QD system as parallel to the z-axis. Additionally, the hybrid system interacts with a squeezed vacuum, E_{squ}. Notably, in the hybrid MNP-QD system, there is no direct tunneling interaction between the MNP and QD. The coupling between the Localized Surface Plasmon (LSP) in the MNP and the exciton in the QD arises from the long-range Coulomb interaction, leading to the formation of a hybrid molecule and facilitating energy transfer . The coupling strength between the MNP and QD is parameterized by g. Other symbols are defined and explained in the main text.

valuable method for effectively addressing the interaction between the MNP and the incident light field [15]. The quasistatic approximation permits the assumption that the incident light field is nearly uniform across the entire MNP sphere. This involves focusing solely on the time-dependent aspect of the oscillating electromagnetic field while neglecting its spatial variations. Within the quasistatic regime, it is efficient to consider the MNP as an ideal dipole. This approach is justified by the fact that the incident field has the capacity to interact solely with the dipole moment of the MNP, excluding higher-order multipoles [16, 17]. When examining the hybrid MNP-QD system, the dipole approximation remains valid as long as the separation distance between the

MNP and QD is sufficiently large. Conversely, the QD can be considered as a pointlike two-level system featuring an excited state $|e\rangle$ and a ground state $|g\rangle$, as depicted in the inset of Figure 2.1. Under the influence of the external laser, the QD detects the superposition field, which composed both the external electric field and the polarized electric field generated by the MNP. Simultaneously, the polarized electric field induced by the QD also influences the MNP, leading to a self-feedback mechanism between these fields within the hybrid MNP-QD system. Within the hybrid system, we explore the optical response of the entire system driven by the external field by employing the dipole-dipole interaction coupling between the LSP in the MNP and the exciton in the QD.

2.1 Total Hamiltonian Of The Metamolecule

In the presence of an external field E_{dri}, the overall Hamiltonian for our hybrid MNP-QD system, within the dipole and rotating-wave approximations, can be expressed as:

$$\hat{H} = \hat{H}_0 + \hat{H}_{int} + \hat{H}_{dri}. \tag{2.1}$$

The initial term on the right-hand side (RHS) of Equation (2.1), corresponding to the unperturbed Hamiltonian($\hat{H}_0$) of the isolated MNP and QD, can be formulated as

$$\mathcal{H}_0 = \hbar\omega_m a^\dagger a + \hbar\omega_x \sigma^\dagger \sigma \tag{2.2}$$

Where ω_m represents the resonance frequency of the surface plasmon in the MNP.The spatial dielectric function of the MNP is defined as $\epsilon_m(\omega) = \epsilon_\infty - \frac{\omega_p^2}{\omega^2+\imath\kappa\omega}$.This leads to the relationship $\omega_m = \frac{\omega_p}{\sqrt{2\epsilon_b+\epsilon_\infty}}$ In this context ω_p denotes the plasma frequency of the metal, ϵ_∞ represents the ultraviolet permittivity of the metal, and ϵ_b stands for the relative permittivity of the homogeneous dielectric in which the hybrid MNP-QD system is embedded.The formulation

for the surface plasmon resonance frequency of the MNP is approximated as

$$\omega_m \approx \sqrt{\omega_p^2 \varepsilon_b + \varepsilon_\infty}$$

The symbols $a^\dagger$ and a represent the creation and annihilation operators for the plasmonic field mode of the MNP, and they adhere to the bosonic commutation relation $[a, a^\dagger] = 1$. For simplicity in notation, we have removed the hat from the operator. $|e\rangle$ and $|g\rangle$ denote the excited and ground states of the two-level QD. $\sigma^\dagger - |e\rangle\langle g|$ and $\sigma - |g\rangle\langle e|$ stand as the dipole raising and lowering operators for the two-level QD, adhering to the fermionic anticommutation relation $\{\sigma^\dagger, \sigma\} - 1$. ω_x signifies the transition frequency of the QD exciton-to-ground states, denoted as $|g\rangle$.The energy of the ground state $|g\rangle$ is designated as zero for the sake of simplicity. Additionally, the zero-point energy for the free MNP, Hamiltonian has been neglected.This is permissible as it only introduces a relative shift and does not alter the dynamics of the MNP-QD system under investigation. The second term on the right-hand side (RHS) of Equation (2.1), connected with the dipole-dipole interaction Hamiltonian (H_{int}) between the MNP and QD, can be expressed as:

$$\mathcal{H}_{int} = \imath\hbar g(a^\dagger \sigma - a\sigma^\dagger) \tag{2.3}$$

Where g represents the coupling strength between the plasmonic field mode of the MNP and the two-level QD, in accordance with the relationship $\hbar g = \mu\varepsilon$. In this context, μ signifies the transition dipole moment of the two-level QD, and it is considered to be real without any loss of generality. The positive-frequency component of the dipole response field, generated by the oscillating surface plasmon mode of the MNP as $e^{-\imath\omega t}$, is sensed by the QD. The expression $E_m^+ = \imath\varepsilon a$ arises from the induced polarization of the MNP under the influence of the external field.Where the expression for $\varepsilon = \frac{\hbar g}{u} = \frac{S_0\hbar}{d^3}\sqrt{\frac{3r_m^3\eta}{4\pi\epsilon_0\hbar}}$ can be derived naturally and coefficient g is defined as $\frac{S_0\mu}{d^3}\sqrt{\frac{3r_m^3\eta}{4\pi\epsilon_0\hbar}}$. The third term on the right-hand side (RHS) of Equation (2.1) considers the dipole interaction between the

MNP and QD with the external driving field E_{drf} as a result:

$$\mathcal{H}_{dri} = -E_0\mu(\sigma^\dagger e^{-\iota\omega_d t} + \sigma e^{\iota\omega_d t}) - E_0(\chi a^\dagger e^{-\iota\omega_d t} + \chi^* a e^{\iota\omega_d t}) \tag{2.4}$$

Here,E_0 represents the amplitude of the external driving field is the ω_d frequency of the external driving field and χ denotes the dipole moment of the MNP.

Effective Hamiltonian to remove the time dependence in the Hamiltonian under the Schrödinger picture, we can transform it into the interaction picture through a unitary operation. To achieve this, we shift the total Hamiltonian (2.1) of the hybrid MNP-QD system into a rotating reference frame (interaction picture) relative to the frequency of the external driving field (ω_d). To accomplish this, the unitary operator is selected as

$$U(t) = e^{-\iota\omega_d t(a^\dagger a + \sigma^\dagger\sigma)} \tag{2.5}$$

Subsequently, employing the unitary transformation formula namely

$$\mathcal{H}_{eff} = U^\dagger(t)H_{tot}U(t) - \iota\hbar U^\dagger(t)\frac{\partial U(t)}{\partial t} \tag{2.6}$$

After performing some algebraic operations, we can ultimately obtain a time-independent effective Hamiltonian for the system in the interaction picture. This is expressed as

$$\mathcal{H}_{eff} = \hbar\Delta_m a^\dagger a + \hbar\Delta_x\sigma^\dagger\sigma + \iota\hbar g(a^\dagger\sigma - a\sigma^\dagger) - E_0\mu(\sigma^\dagger + \sigma) - E_0(\chi a^\dagger + \chi^* a) \tag{2.7}$$

Here, the symbol $\Delta_m = \omega_m \quad \omega_d$ signifies the detuning of the plasmon resonance frequency ω_m of the MNP from the frequency ω_d of the external driving laser.. Here, $\Delta x = \omega_x - \omega_d = \omega_m + \Delta - \omega_d$ indicates the detuning of the exciton resonance frequency ω_x of the two-level QD from the frequency ω_d of the external driving laser.In this context, the symbol $\Delta = \omega_x - \omega_m$ denotes the detuning of the exciton resonance frequency ω_x of the two-level QD from the plasmon resonance frequency ω_m of the MNP.

2.2 The Lindblad Master Equation

The Hamiltonian (2.1) mentioned above pertains to a closed quantum system, and it does not account for any losses within the MNP-QD system stemming from interactions with the external environment. In reality, considering the influence of the environment or reservoir involves coupling the system with the environment, resulting in the construction of an open quantum system characterized by irreversible dynamics. In this study, our primary focus is on the hybrid system interacting with a squeezed vacuum, ω_{squ} (refer to Fig. 2.1). This interaction is facilitated through the application of the unitary squeezing operator $S(\xi) - \exp\left[\frac{1}{2}(\xi^* a^2 - \xi a^{\dagger 2})\right]$, on the vacuum state interaction specifically involves the use of a squeezed vacuum, distinct from the vacuum or thermal reservoir [18].Here, $\xi = re^{i\phi}$ denotes the squeezing parameter, where the squeezing strength r,characterizes the degree of squeezing with a value range of $0 \leq r < \infty$. The squeezing angle, ϕ, represents the direction of squeezing with a value range of $0 \leq \phi \leq 2\pi$. To encompass incoherent processes and fully characterize the dynamics of the MNP-QD system using the density matrix operator ρ, we can utilize the Lindblad master equation under the Born-Markovian and secular approximations [19].

$$\frac{d\rho}{dt} - -\frac{\iota}{\hbar}[H,\rho] + L_{field}(\rho) + L_{QD}(\rho) \tag{2.8}$$

Where

$$\begin{aligned} L_{\text{field}}(\rho) - & \frac{N\kappa}{2}(2a^{\dagger}\rho a - aa^{\dagger}\rho - \rho aa^{\dagger}) \\ & + \frac{(N+1)\kappa}{2}(2a\rho a^{\dagger} - a^{\dagger}a\rho - \rho a^{\dagger}a) \\ & - \frac{M\kappa}{2}(2a\rho a - aa\rho - \rho aa) \\ & - \frac{M^*\kappa}{2}(2a^{\dagger}\rho a^{\dagger} - a^{\dagger}a^{\dagger}\rho - \rho a^{\dagger}a^{\dagger}) \end{aligned} \tag{2.9}$$

and

$$\begin{aligned} I_{QD}(\rho) =& \frac{N\gamma}{2}(2\sigma^{\dagger}\rho\sigma - \sigma\sigma^{\dagger}\rho - \rho\sigma\sigma^{\dagger}) \\ &+ \frac{(N+1)\gamma}{2}(2\sigma\rho\sigma^{\dagger} - \sigma^{\dagger}\sigma\rho - \rho\sigma^{\dagger}\sigma) \\ &- \frac{M\gamma}{2}(2\sigma\rho\sigma - \sigma\sigma\rho - \rho\sigma\sigma) \\ &- \frac{M^{*}\gamma}{2}(2\sigma^{\dagger}\rho\sigma^{\dagger} - \sigma^{\dagger}\sigma^{\dagger}\rho - \rho\sigma^{\dagger}\sigma^{\dagger}) \\ &+ \frac{\gamma_{dph}}{2}(2\sigma^{\dagger}\sigma\rho\sigma^{\dagger}\sigma - \sigma^{\dagger}\sigma\rho - \rho\sigma^{\dagger}\sigma) \end{aligned} \tag{2.10}$$

In the above context, the impact of the squeezed vacuum field is denoted by the parameters N, M and ϕ respectively.These parameters are intricately linked to the squeezing parameter $\xi = re^{i\phi}$ in the following manner [19] $N = \sinh^2(r)$ and $M - \sinh(r)\cosh(r)e^{-i\phi}$, where N represents the mean number of photons in the squeezed vacuum, and M signifies the intensity of the two-photon correlation [20].The squeezed vacuum reservoir transitions into a standard vacuum reservoir when $N - |M| - 0$. Furthermore, it transforms into a typical thermal radiation reservoir when $N = 0$ and $|M| = 0$ [21]. To maximize the effects of squeezing, we make the assumption that $|M| - \sqrt{N(N+1)}$, representing the maximum permissible value for $|M|$ [22]. Moving forward, we will investigate the impact of the squeezed vacuum on the optical characteristics of the hybrid MNP-QD system, considering the squeezing strength (r) and the squeezing phase (ϕ) as the variables.In this context, $\kappa = \kappa_r + \kappa_{nr}$ and γ represent the decay rates of the MNP and the QD, respectively. κ_r accounts for radiation loss due to radiation to the far field, κ_{nr} addresses nonradiation loss caused by Ohmic loss, and γ_{dph} is the dephasing rate of the QD.

2.3 Heisenberg Equation Of Motion

Starting from the quantum master equation, we can derive the coupled equation of motion for the expectation values of the MNP plasmonic field.

$$\frac{\partial a}{\partial t} - \frac{\partial}{\partial t}\mathrm{Tr}(a\rho) - \mathrm{Tr}\left(a\frac{\partial}{\partial t}\rho\right) \tag{2.11}$$

By substituting Eqs (2.7) and (2.8) into Eq. (2.11) and applying the relevant commutation relations, we can determine:

$$\langle\frac{\partial a}{\partial t}\rangle = -(i\Delta_m + \frac{\kappa}{2})\langle\, a\rangle + g\langle\sigma\rangle + \frac{iE_0\chi}{\hbar} \tag{2.12}$$

Similarly, following the same approach as before, we can derive the coupled equation of motion governing the expectation value of the excitonic transition operator, which determines the QD polarization, as

$$\frac{\partial\sigma}{\partial t} = \frac{\partial}{\partial t}\mathrm{Tr}(\sigma\rho) = \mathrm{Tr}\left(\sigma\frac{\partial}{\partial t}\rho\right) \tag{2.13}$$

Through a series of calculations based on the derived equations, we obtain:

$$\begin{aligned}\langle\frac{\partial\sigma}{\partial t}\rangle = &-\left(i\Delta_x + (2N+1)\frac{\gamma}{2} + \frac{\gamma_{dph}}{2}\right)\langle\sigma\rangle - g\langle a\rangle \\ &+ 2g\langle\, a\sigma^\dagger\sigma\rangle + \frac{iE_0\mu}{\hbar}(1 - 2\langle\sigma^\dagger\sigma\rangle) - M^*\gamma\langle\sigma^\dagger\rangle\end{aligned} \tag{2.14}$$

From Eq. (2.12), we can obtain the analytical solution for a in the steady state by equating the left side of Eq. (2.12) to zero.

$$\langle a\rangle = \frac{g\langle\sigma\rangle}{i\Lambda_m + \frac{\kappa}{2}} + \frac{iE_0\chi}{\hbar(i\Lambda_m + \frac{\kappa}{2})} \tag{2.15}$$

In the regime of a weak driving field, where the number of excitons in the QD can be approximately neglected, i.e., $\langle\sigma^\dagger\sigma\rangle \ll 1$, we can obtain

$$\langle\sigma\rangle = \frac{-g\langle a\rangle + \frac{iE_0\mu}{\hbar} - M^*\gamma\langle\sigma^\dagger\rangle}{i\Delta_x + (2N+1)\frac{\gamma}{2} + \frac{\gamma_{dph}}{2}} \tag{2.16}$$

The parameters g and χ is given as:

$$g = \frac{S_\alpha \mu}{d^3}\sqrt{\frac{3r_m^3\eta}{4\pi\epsilon_0\bar{h}}} \tag{2.17}$$

and

$$\chi = -i\epsilon_b\sqrt{12\eta\epsilon_0\pi\bar{h}r_m^3} \tag{2.18}$$

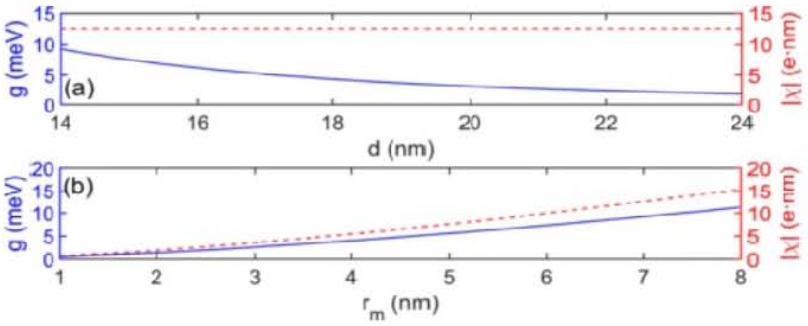

Figure 2.2: The graphs depict the coupling strength g between the MNP and QD, along with the modulus of the complex dipole moment χ of the MNP. In panel (a), these parameters are examined concerning the MNP-QD center-to-center distance d when $r_m = 7$ nm. Panel (b) explores the coupling strength g and the modulus of χ as functions of the MNP radius r_m when $d = 14$ nm. All graphs maintain consistency with specific system parameters: $S_\alpha = 2$, $\mu = 0.7$ e nm, $\varepsilon_b = 1$, $\omega_p = 7418.71$ meV, $\kappa = 53.28$ meV, and $\varepsilon_\infty = 4.6$.The blue solid line corresponds to the left axis, while the dashed red line corresponds to the right axis in each panel

2.4 Quantum Polarization Operator

After determining both g and χ, we can derive the complete expression for the total polarization operator P as

$$P = \chi^* a + \mu\sigma. \tag{2.19}$$

The resonance fluorescence of the hybrid MNP-QD system is manifested through the power spectral density. By utilizing the first-order correlation function $\langle P^{\dagger}(\tau)P(0)\rangle$,the corresponding power spectral density is defined as the Fourier transform of the first-order correlation function [19, 23].

$$S(\omega) = \int_{\infty}^{+\infty} \langle P^{\dagger}(\tau)P(0)\rangle e^{-i\omega\tau}\, d\tau. \tag{2.20}$$

In the limit of a steady state ($t \to \infty$) we assess the fluorescence spectrum $S(\omega)$ utilizing the quantum regression theorem [24]. The intricate nature of the analytical results necessitates numerical solutions of the full master equation (2.8). It's important to highlight that all computations are performed in the rotating frame at the driving field frequency ω_d.

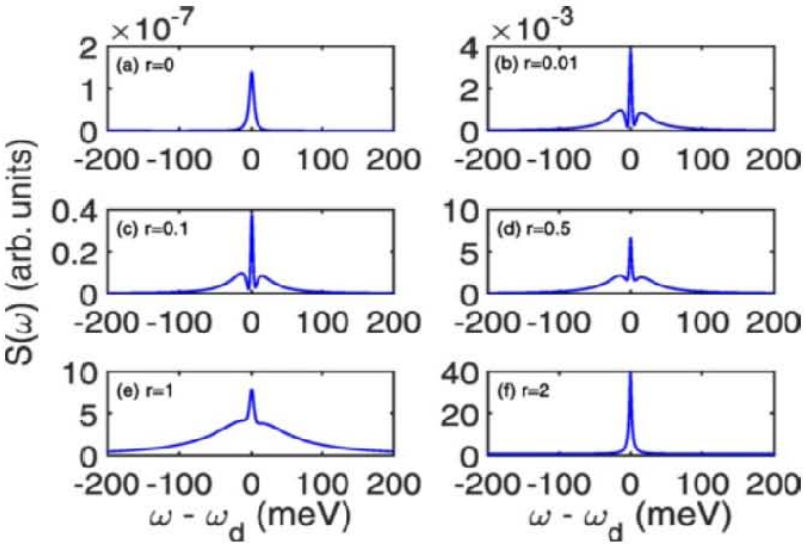

Figure 2.3: The fluorescence spectra are presented for a set of parameters $S_{\alpha} = 2$, $\mu = 0.7$ e nm, $r_m = 7$ nm, $d = 14$ nm, $\epsilon_b = 1$, $\gamma = 0.05$ meV, $\gamma_{\mathrm{dph}} = 0.005$ meV, $\phi = 0$, $I = 1$ W/cm², $\Lambda_m = 0$ meV, and $\Lambda = 0$ meV. The six panels illustrate distinct squeezing amplitudes: (a) $r = 0$; (b) $r = 0.01$; (c) $r = 0.1$; (d) $r = 0.5$; (e) $r = 1$; and (f) $r = 2$.

Chapter 3

Metal-Nano-Particale As Nano-Ring

3.1 The MNP Nano-Ring

Now, let's shift our focus to arrangement the metal nano particles in a ring configuration, which work like a magnet in the visible light range [?]. Our goal is to understand the quantum side of this setup, basically, how these tiny particles behave when we bring in the special molecule we talked about before. This special addition is expected to bring out some interesting changes, like adjusting how our magnet works and making it respond in a not-so-straightforward manner. To determine the μ or ϵ of a metamaterial, it's a standard approach to separate its response to either an electric or magnetic field, depending on the specific incident field used. Now we calculate μ and ϵ using a specific excitation method, these properties effectively capture how the metamaterial responds to any form of incident field.Hence, our investigation will specifically target extracting and understanding the magnetic behavior of the ring [?] To achieve this, we apply a high-frequency magnetic field along the normal axis of the ring, as illustrated in (Fig 3.1). Consequently, the MNPs undergo the following electric field.

$$E_0 = \frac{i\omega_d \mu_0 R H_0}{2}\phi \tag{3.1}$$

Induced by the time-varying incident field $H = H_0 e^{-i\omega t}\hat{z}$, where R de-

notes the radius of the ring, ω_d represents the frequency of the driving field, and $\hat{R}$, $\hat{\theta}$, and $\hat{z}$ serve as unit vectors within the cylindrical coordinate system. The displacement field generated within each magnetic nanoparticle is similarly aligned along the azimuthal direction. Due to this symmetry, there is no net electrical response, enabling us to concentrate specifically on the magnetic response of the system. A circular displacement field current is initiated, functioning as a magnetic dipole whose strength is determined by [?].

$$m = \frac{-i\omega P_{MNP} N R}{2} \tag{3.2}$$

Where N denotes the count of electric dipoles within the ring and P_{MNP} represents the dipole moment of an individual magnetic nanoparticle. The configuration illustrated in Figure 3.1 emphasizes our consideration of a material displaying magnetic response exclusively along the $\hat{z}$ direction.Therefore, the material demonstrates anisotropic behavior.To achieve isotropic behavior across all directions, it is recommended to employ Achieving this involves creating a cubic lattice consisting of three orthogonal arrays of nanorings for the material. This objective can be accomplished within a face-centered cubic lattice, enabling the integration of up to four distinct nanoring orientations within a single unit cell. [?]. Moreover,we specifically focus on the scenario where N = 4, as this represents the minimum number of magnetic nanoparticles within the ring. This choice ensures that the magnetic dipolar response takes precedence over higher-order multipoles [?]. It is essential to preserve the accuracy of characterizing the metamaterial's magnetic response by considering the effective permeability parameter.(μ_{eff}), We proceed to derive the expression, as detailed in the reference [?].We initiate the calculation of the dipole moment for an individual magnetic nanoparticle within a quantum framework. While, strictly speaking, a quantum approach may not be essential as the process is fundamentally classical, we establish the quantum formalism at this stage for future integration of MNP-QD metamolecules into the ring in the subsequent section. Consequently, the equations of motion derived through this framework remain applicable even in the classical regime.

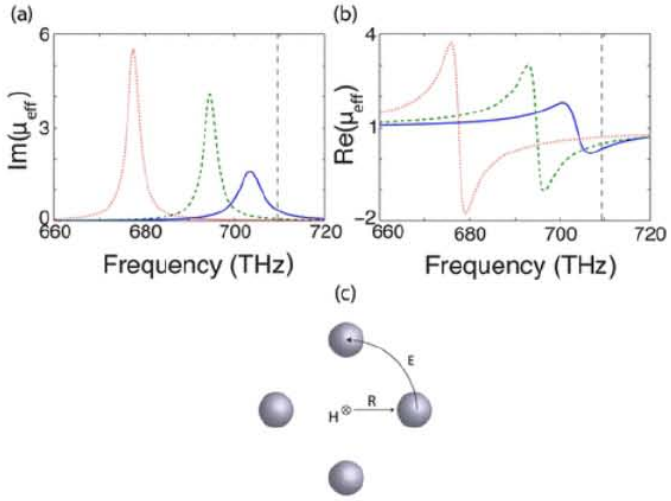

Figure 3.1: MNP nanoring

3.2 Hamiltonian Of The MNP Nano-ring

The Hamiltonian of the MNP nanoring is expressed as follows.

$$\hat{H} = \hat{H}_0 + \hat{H}_{int} + \hat{H}_{dri}. \tag{3.3}$$

where

$$\hat{H}_0 = \sum_{n=0}^{N-1} \hbar\omega_m \hat{a}_n^\dagger \hat{a}_n \tag{3.4}$$

$$\hat{H}_{\text{dri}} = -E_0 \sum_{n=0}^{N-1} (\chi^* \hat{a}_n e^{-i\omega_d t} + \chi \hat{a}_n^\dagger e^{i\omega_d t}) \tag{3.5}$$

The frequency of inter-magnetic nanoparticle coupling is denoted as J_{nm}. J_1 for nearest-neighbor coupling, and J_2 for next-nearest-neighbor coupling it is denoted as

$$J_{1(2)} = -12\pi\epsilon_0\epsilon_b^2 r^3 \eta Q_{1(2)} \tag{3.6}$$

The term $Q_{1(2)}$ represents the scalar interaction between closest (next-closest) neighborir magnetic nanoparticles.This interaction term incorporates both near-field and radiative interactions. [**?**].We express as

$$Q_1 - \frac{e^{i\sqrt{2}kR}}{16\sqrt{2}\pi\varepsilon_0\epsilon_b R^5}(-2k^2R^4 + 3R^2(1 - ik\sqrt{2R})), \tag{3.7}$$

$$Q_2 = \frac{e^{i2kR}}{128\pi\varepsilon_0\epsilon_b R^5}(-16k^2R^4 + 4R^2(1 - i2kR)), \tag{3.8}$$

Here, k represents the wave vector of light, defined as, $k = \omega\sqrt{\varepsilon_0\varepsilon_b\mu_0\mu_b}$.

3.3 Expectation Values Of The MNP Nanoring

The complete system Hamiltonian, we can derive the equation of motion, as $\hat{a}_n$. Specifically, for N=4 :

$$\langle\dot{\hat{a}}_n\rangle = -(i\Delta_m + \frac{\gamma_m}{2})\langle\hat{a}_n\rangle - iJ_1\langle\hat{a}_{n+1}\rangle - iJ_1\langle\hat{a}_{n-1}\rangle - iJ_2\langle\hat{a}_{n+2}\rangle + \frac{i\chi E_0}{\hbar} \tag{3.9}$$

Solving the set of coupled equations in the steady state is straightforward due to the system's inherent symmetry, resulting in uniform expectation values for each dipole. Utilizing equations (2.18) and (2.19), we can express the dipole moment of an individual magnetic nanoparticle.

$$P_{\text{MNP}} = \left(-\frac{|\chi|^2\omega\mu_0 RH_0}{2\hbar(i\Delta_m + \frac{\kappa_0}{2})}\right)\left(1 + \frac{i(2J_1 + J_2)}{i\Delta_m + \frac{\kappa_0}{2}}\right)^{-1} \tag{3.10}$$

3.4 Effective Permeability Of The MNP Nanoring

Subsequently, by employing Eq. (3.2), we can determine the magnetic polarizability of an individual nanoring, denoted as $\alpha_m = \frac{m}{H_0}$. The μ_{eff} of system, often referred to as the metamaterial, can be determined through the application of

the Maxwell-Garnett mixing formula [? ?].

$$\mu_{\text{eff}} = 1 + \frac{1}{N_d^{-1}(\alpha_m^{-1} + i\frac{k^3}{6\pi}) - 1/3} \tag{3.11}$$

The parameter N_d signifies the volume of nanorings within the composite system. The inclusion of the im term in the denominator is relevant only when the nanorings are integrated into a regular three-dimensional array. In such a configuration, the radiative damping of the magnetic dipole is nullified.[?].

In Fig. 3.1, we illustrate the μ_{eff} of a metamaterial featuring nanorings with 2, 3, and 4 magnetic nanoparticle (MNP) inclusions. While it is emphasized that the effective permeability is physically meaningful only for N=4, we include plots for N=1,2,3 to demonstrate the influence of a single MNP (indicated by the vertical dashed line). Both Fig. 3.1 (a) and (b) showcase the material's resonance properties, with panel (b) displaying negative real values. The MNP nanoring is characterized by the parameters from Ref. [?].

Chapter 4

Unite Cell Of Quantum Metamaterials

4.1 Metal-Nanoparticle - Quantum Dot Nano-Ring

Now, we're switching things up a bit. Instead of the original MNP, we're using a combination of MNP and QD meta molecules in our nano-ring design as shown in Fig 4.1 (c). In this scenario, two magnetic dipoles are triggered by the incoming magnetic field: one created by the MNP ring and the other by the QD ring. Once more, we employ Eq (3.12) to compute the effective permeability of a metamaterial comprised of these MNP-QD nano-rings. However, in this instance, we need to address the presence of two magnetic dipole excitation's, while also considering the interactions between MNPs and QDs.

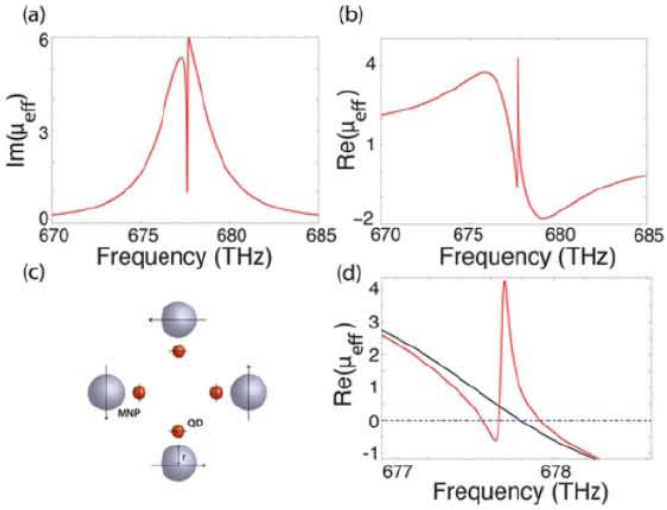

Figure 4.1: MNP-QD Nano-Ring and its Results

4.2 Hamiltonian of the MNP-QD Nano-Ring

The Hamiltonian of the $MNP-QD$ nano-ring is expressed as follows.

$$\hat{H} = \hat{H}_0 + \hat{H}_{int} + \hat{H}_{dri}. \tag{4.1}$$

Where the Individule terms are

$$\begin{aligned} \hat{H}_{\text{int}} = & \sum_{n,m=0}^{N-1} \hbar J_{nm}(\hat{a}_n^\dagger \hat{a}_m + \hat{a}_m^\dagger \hat{a}_n), \quad n \neq m \\ & + \sum_{n,m=0}^{N-1} \hbar I_{nm}(\hat{\sigma}_n^\dagger \hat{\sigma}_m + \hat{\sigma}_m^\dagger \hat{\sigma}_n), \quad n \neq m \\ & + \sum_{n,m=0}^{N-1} i\hbar g_{nm}(\hat{a}_n^\dagger \hat{\sigma}_m + \hat{a}_n \hat{\sigma}_m^\dagger), \quad n \neq m \end{aligned} \tag{4.2}$$

$$\hat{H}_{\text{dri}} = -E_0 \sum_{n=0}^{N-1} (\chi^* \hat{a}_n e^{-i\omega_d t} + \chi \hat{a}_n^\dagger e^{i\omega_d t}) - E_0 \mu \sum_{n=0}^{N-1} (\hat{\sigma}_n e^{-i\omega_d t} + \hat{\sigma}_n^\dagger e^{i\omega_d t}) \tag{4.3}$$

4.3 Expectation Values Of The MNP-QD Nano-Ring

Initially, we're figuring out how materials respond when exposed to a weak magnetic field. To tackle this, we're working with steady-state MB matrix equations, taking into consideration the unique features of each location in the system.

$$A\bar{a} = B\bar{\sigma} + \bar{c} \tag{4.4}$$

$$D\bar{\sigma} = B\bar{a} + \bar{e} \tag{4.5}$$

Where the $\bar{\sigma}$ and $\bar{a}$ are vectors. Wher $\bar{\sigma}$ and $\bar{a}$ at each site in the $MNP - QD$ nano-ring is

$$\bar{a} = \begin{pmatrix} \langle \hat{a}_1 \rangle \\ \langle \hat{a}_2 \rangle \\ \langle \hat{a}_3 \rangle \\ \langle \hat{a}_4 \rangle \end{pmatrix}, \bar{\sigma} = \begin{pmatrix} \langle \hat{\sigma}_1 \rangle \\ \langle \hat{\sigma}_2 \rangle \\ \langle \hat{\sigma}_3 \rangle \\ \langle \hat{\sigma}_4 \rangle \end{pmatrix} \tag{4.6}$$

Where the matrix A represents the $MNP - MNP$ interactions in the $MNP - QD$ nano-ring which we can writer as

$$A = \begin{bmatrix} i\Delta_m + \frac{\kappa_m}{2} & iJ_1 & iJ_2 & iJ_1 \\ iJ_1 & i\Delta_m + \frac{\kappa_m}{2} & iJ_1 & iJ_2 \\ iJ_2 & iJ_1 & i\Delta_m + \frac{\kappa_m}{2} & iJ_1 \\ iJ_1 & iJ_2 & iJ_1 & i\Delta_m + \frac{\kappa_m}{2} \end{bmatrix} \tag{4.7}$$

Here, J_n represents the MNP-MNP coupling frequency, which has been detailed in Chapter 2 and the matrix D represents the $QD - QD$ interactions in the $MNP - QD$ nano-ring, given as

Where the I_1 , I_2 denote the closer and next-closer neighbor coupling frequencies, respectively, which is defined as

$$I_1(2) = \frac{\mu^2}{\hbar} Q_{1(2)} \tag{4.8}$$

The matrix B represents the coupling between MNP and QD, called coupling matrix which is define as

In this context, the coupling frequency g_1 pertains to interactions between MNP and QD when they are on the same site. On the other hand, g_2 corresponds to the coupling between an MNP and its neighboring QD located at the next nearest site. Referring to Figure 4.1(c), it is evident that the interactions between same-site and next-nearest neighbors are transverse, as indicated by the value S = -1. Because of the external electric field in the azimuthal direction stimulating the ring, the QD located on the same site and those at the neighbor site relative to each MNP are compelled to move in opposite directions. Consequently, their oscillations are in anti-phase, a characteristic reflected by the negative values within the matrix. We observe that the next-nearest neighbor QD plays a role in diminishing the impact of the same-site QD on each MNP. Fano interference still occurs due to the stronger same-site interaction frequency. Likewise, the QDs situated as nearest neighbors to a MNP also exhibit with differents relationship. In such scenario, their interaction frequency is identical, resulting in a cancellation of their combined effect on the MNP. Lastly, the vectors $\bar{C}$ and $\bar{E}$ symbolize the E_{dri} forces acting on the $MNPs$ and QDs, influenced by the induced E field.

The different sizes of the MNP and QD nano-rings, with sizes represented by R_1 and R_2 , we can use these equations to figure out how each MNP and QD in the nano-ring behave in terms of their dipole moment.

$$P_{\mathrm{MNP}} = \chi^* \bar{a}_1 = \chi^* \left(A + B(D^{-1})B\right)^{-1} \left(B(D^{-1})\bar{e} + \bar{c}\right), \tag{4.9}$$

$$P_{\mathrm{QD}} = \mu \bar{\sigma}_1 = \mu \left(D + B(A^{-1})B\right)^{-1} \left(B(A^{-1})\bar{c} + \bar{e}\right). \tag{4.10}$$

4.4 The Magnetic Polarizability Of the $MNP - QD$ Nano-Ring

The procedure which is use in chapter no.2 we calculate the magnetic dipole of both the MNP and QD rings.The magnetic polarizability of the entire $MNP - QD$ nano-ring can be determined through the following expression $\alpha_m = \frac{m_{\mathrm{MNP}} + m_{\mathrm{QD}}}{H_0}$.

4.5 Effective Permeability Of MNP-QD Nano-Ring

To calculate the (μ_{eff}), we can utilize Equation (3.12) to compute the (μ_{eff}) of a metamaterial constructed from $MNP - QD$ nano-rings. Where the meta-material's (μ_{eff}) is illustrated in Figure 4.1(a), (b). Because of the red-shift observed in the magnetic resonance of the MNP ring, as detailed in chapter 3 (refer to Fig. 3.1), adjustments were made to red-shift the QD resonances. This modification was implemented to facilitate Fano interference. The MNP ring possesses a radius of R1 = 38 nm, whereas the QD ring has a radius of R2 = 6 nm. Consequently, the separation between the MNP and QD on the same site is d = 32 nm, a value consistent with the MNP-QD molecule discussed in Chapter 2. However, it is evident that the Fano interference exhibited in the effective permeability is more pronounced compared to what is observed in the polarizability of an individual MNP-QD molecule (refer to Fig. 2.1). This phenomenon arises from the interactions between multiple QDs in the nano-ring and each MNP, whether through direct interaction or mediation via MNP-MNP interactions. In Figure 4.1(d), we illustrate the transformation of the real part of permeability from positive to negative by introducing QDs in the nano-ring design, achieved through Fano interference. Although the magnitude of the Fano-affected $\text{Re}(\mu_{\text{eff}})$, when negative, may not be exceptionally large, it is contingent upon the magnetic resonator's strength. Nevertheless, the resonance strength can be amplified by augmenting the number of sites in the ring [**?**].

It's clear that integrating QDs into the MNP nanoring has effectively transposed the distinctive Fano line shape of the meta-molecule onto the (μ_{eff}) of the resulting meta-material. This means we have the power to adjust when certain effects happen. For example, in Figure 4.1(d), we can see that at a specific point where MNP and QD interact, a dip in the response causes a -ve effect, giving us more control over how the material behaves. Therefore, by actively adjusting the detuning between the $MNPs$ and the QDs, it becomes possible to change the frequency at which the meta-material exhibits -ve permeability, as demonstrated in Figure (4.2). Whever a trade-off for this adaptability: as the QDs move away from the magnetic resonance, the range of frequencies show-

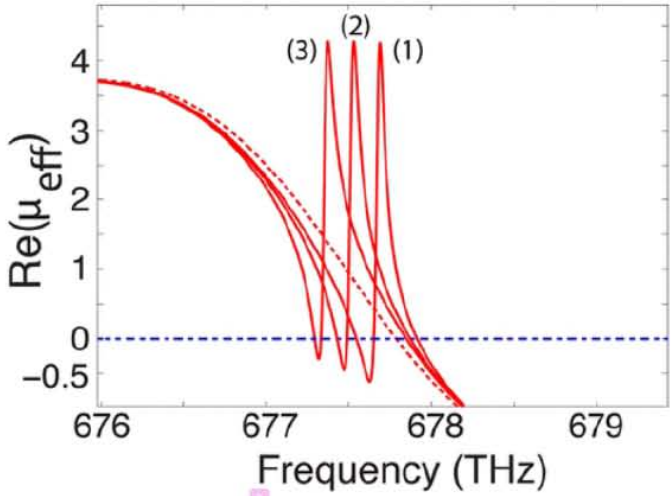

Figure 4.2: Tunability Of the MNP-QD

casing the effect becomes narrower. The bandwidth (δ) of the dip decreases from 0.04 THz to 0.02 THz as we shift the QD away from the resonance of the MNP nano-ring. Despite reduction, still stands when compared by experiments with cold rubidium atoms in Electromagnetically Induced Transparency (EIT), where the observed bandwidth is a mere 50 MHz [**?**].

4.6 Fano Rasonance

Fano Resonance occurs when an allowed discrete energy state interferes with an overlapping continuum of states, leading to an asymmetric line-shape in the resulting spectrum show in Fig (4.3). Our calculations have been restricted of the context of a weak field. However, to delve into the nonlinear properties of the nano-ring metamaterial, we must now consider the influence of a strong driving field.In the scenario where the MNP-QD meta molecule experiences strong driving from an intense light field, there is a profound alteration in its optical scattering properties. The driving field saturates the QD, leading to the disappearance of its interaction with the MNP field.The emergence of this non-

linear Fano effect is beyond the predictive capacity of classical or semiclassical theories. It has been explored in prior studies of isolated $MNP - QD$ systems and more recently observed in quantum-well structures [**? ?**]. In Figure 4.3, we deliberately chose parameters for our investigation to demonstrate this particular effect in a single $MNP - QD$ system within the nano-ring. Both the MNP and the QD experience the same external field. Progressing from the top row to the bottom row, it becomes apparent that with increasing field intensity, the characteristic Fano dip in the meta-molecule's polarizability diminishes due to the saturation of the QD population. These findings were obtained by numerically solving the full master equation, which entails solving the eigenproblem.

$$\hat{\mathcal{L}}(\hat{\rho}_{SS}) = 0 \tag{4.11}$$

In this context, $\hat{\rho}_{SS}$ denotes the density matrix of the system in the Non-Equilibrium Steady State (NESS). The difficulty stems from the unbounded dimensions of the bosonic MNP field mode, which is characterized by an infinite Hilbert space. To account for the non-classical behavior of the system, each dimension of the MNP field's Hilbert space is truncated with a lower bound set at $d = 15$. Resolving this challenge aligns with the quantum optics toolkit established by Tan. [**?**].

While our nano-ring consists of a minimum of 4 $MNPs$, resulting in a vast combined Hilbert space, the current computational demands limit a comprehensive exploration of the saturation of the nanoring. Despite these computational constraints, if the QD in the $MNP - QD$ metamolecule reaches saturation, a similar saturation is logically expected when coupled to the $MNPs$ in the nanoring. The integration of QDs into the MNP nanoring induces a negative permeability at their resonance frequency, as depicted in Fig. 4.1 and Fig. 4.2. Consequently, if the QD is saturated by a distinct control field, the permeability could be manipulated and varied with light intensity, transitioning between positive and negative values. In future investigations, techniques from many-body quantum systems may be combined with our formalism to facilitate more manageable computations [**?**].

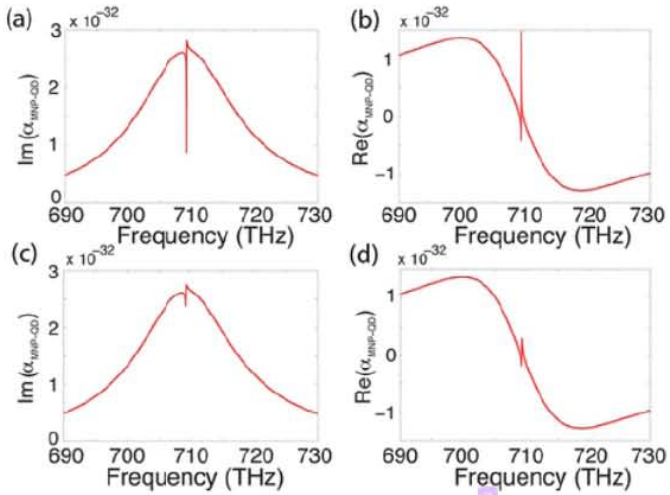

Figure 4.3: Examining the nonlinear characteristics of the $MNP-QD$ metamolecule, we compare the imaginary (a), (c) and real (b), (d) components of the polarizability. The upper row illustrates the response to a weak external driving field $E_0\mu = 0.0001, \text{meV}$, while the lower row demonstrates the behavior under a strong driving field $E_0\mu = 0.1, \text{meV}$. In both scenarios, the $MNP-QD$ detuning is fixed at $\Delta = 0.195 \times 10^{15}, \text{rad s}^{-1}$.

Chapter 5

Conclusion

When combined with two-level quantum dot systems, the quantum optical framework designed for the negative permeability metamaterial has revealed important new information. Notably, the overall magnetic properties of the metamaterial have been observed to be influenced by the detection of Fano interference inside the hybrid structure of metamaterial and quantum dots. This phenomena has been used to control the metamaterial's characteristics, demonstrating possible real-world uses. Furthermore, the study of nonlinear Fano effects at high driving conditions has uncovered fascinating dynamics in the nano-ring. On the other hand, difficulties have surfaced in obtaining autonomous control over the distributed fields of electric and magnetic energy. Future studies aiming at combining magnetic nanoring resonators with a broadband negative permittivity background are now necessary as a result of this. Control over the metamaterial's refractive index and dynamic modifications of its magnetic response may be made possible by such an integration. In metal nanoparticle (MNP) fields, the significance of taking realistic damping into account has been emphasized. Various potential solutions have been suggested, such as including gain materials or alternative nanostructures. Strongly polarized plasmonic nanostructures that are complex have been suggested as workable substitutes that preserve the qualitative aspects of the theoretical framework. It has been shown in a different study that it is possible to engineer and control the optical fluorescence spectra of the MNP-QD molecule by using a quantum-squeezed reservoir. The results

have demonstrated the tunability of spectrum characteristics, including fluorescence quenching, amplification, narrowing, and Fano-type resonance fluorescence. The ability to modify the quantity and orientation of fluorescence peaks has been highlighted, indicating possible uses of the hybrid MNP-QD system in optical modulation, lasing, switching, and sensing.

Fano Resonance in Quantum Metamaterials

ORIGINALITY REPORT

8%	7%	8%	0%
SIMILARITY INDEX	INTERNET SOURCES	PUBLICATIONS	STUDENT PAPERS

PRIMARY SOURCES

1	Shuting Shen, Zhiming Wu, Jiahua Li, Ying Wu. "Insights into Fano-type resonance fluorescence from quantum-dot–metal-nanoparticle molecules with a squeezed vacuum", Physical Review A, 2021 Publication	2%
2	hdl.handle.net Internet Source	2%
3	dx.doi.org Internet Source	2%
4	K. R. McEnery, M. S. Tame, S. A. Maier, M. S. Kim. "Tunable negative permeability in a quantum plasmonic metamaterial", Physical Review A, 2014 Publication	1%
5	spiral.imperial.ac.uk Internet Source	1%

Exclude quotes	On	Exclude matches	< 1%

Exclude bibliography On

Fano Resonance in Quantum Metamaterials

GRADEMARK REPORT

FINAL GRADE

/0

GENERAL COMMENTS

PAGE 1

PAGE 2

PAGE 3

PAGE 4

PAGE 5

PAGE 6

PAGE 7

PAGE 8

PAGE 9

PAGE 10

PAGE 11

PAGE 12

PAGE 13

PAGE 14

PAGE 15

PAGE 16

PAGE 17

PAGE 18

PAGE 19

PAGE 20

PAGE 21